Far-infrared foreign and self-broadened rotational linewidths of high-temperature water vapor

R. A. Cheville and D. Grischkowsky

School of Electrical and Computer Engineering and Center for Laser and Photonics Research, Oklahoma State University, Stillwater, Oklahoma 74078

Received August 30, 1998; revised manuscript received November 4, 1998

We report what is believed to be the first measurement of rotational line broadening of high-temperature water vapor for transition frequencies that range from 1.0 to 2.5 THz (33 to 83 cm^{-1}). Water-vapor rotational transitions were measured in a near-stoichiometric propane–air flame at 1490 K with THz time-domain spectroscopy. Linewidths were measured for 29 pure rotational transitions in both ground vibrational and $\nu_2 = 1$ vibrational levels with lower state energies ranging from 80 to 2390 cm^{-1}. Measured widths show a dependence on rotational state energy that roughly follows a thermal distribution with variation between various J, K_a, K_c rotational quantum numbers. © 1999 Optical Society of America [S0740-3224(99)01002-4]

OCIS codes: 300.6240, 300.6270, 300.6390, 320.7150.

1. INTRODUCTION

The universality of water makes it one of the most important and interesting species for spectroscopic investigation. The spectroscopy of water vapor has wide application in a multitude of diverse fields. These range from heat balance in the the terrestrial atmosphere and associated climatological modeling,[1] to practical electromagnetic propagation calculations,[2] to astronomy, owing to observations of water emissions from the Sun[3,4] and observation of water masers in interstellar[5] astronomy.

Accurate modeling of water-vapor absorption over frequency intervals from the radio wave to the ultraviolet spectral regions is determined by knowledge of three factors: line center, line strength, and line broadening. Typically, line centers are known to great accuracy, strengths somewhat less so, and line broadening the least. This is due to the influence that external variables such as temperature and the local molecular environment have on line strengths and, to an even greater extent, on linewidths.

Of the work done on self-broadening and foreign gas broadening of water vapor, the bulk of the treatments have been predominantly theoretical. The experimental work that supports the theoretical calculations is generally over a limited range of conditions. The majority of experimental work has been carried out under temperature conditions near 300 K and over the range of several hundred to several thousand wave numbers, where Fourier-transform IR spectrometers perform well. Experimental results have not been available previously at high temperatures in the FIR region of the spectrum where the thermal background noise limits accurate measurements.

Here we report what we believe are the first measurements in the submillimeter spectral region of collisionally broadened linewidths at high temperatures. Water vapor generated in a propane–air flame is observed over a broad spectral bandwidth from 1 to 2.5 THz (33 to 83 cm^{-1}) with THz time-domain spectroscopy (THz-TDS). This coherent technique is blind to the thermal background in the FIR region of the spectrum. We observe more than 40 pure rotational lines in ground and $\nu_2 = 1$ vibrational levels. Comparing the relative strengths of the absorption with that at room temperature allows for temperature determination. To determine the collisionally broadened linewidth, the lines are fit numerically to a Lorentzian profile convolved with a sinc function that is determined by the measurement window.

2. EXPERIMENT

The experimental technique of THz-TDS directly measures the time-resolved electric-field amplitude of a nearly single-cycle subpicosecond electromagnetic pulse. For our measurements two electromagnetic pulse shapes are measured, the input (reference) pulse and the propagated pulse, which has changed shape as a result of its passage through the sample under study. Because both amplitude and phase information are obtained in the time-domain measurement, Fourier analyses of input and propagated pulses allow for extraction of the frequency-dependent absorption and dispersion of the sample over a bandwidth that extends from 100 GHz to beyond 3 THz.

The experimental system used for THz-TDS of active flame regions[6,7] is shown in Fig. 1(a). THz pulses are generated by the ultrashort laser pulses incident on the optoelectronic source chip. The generated THz beam is collimated by a silicon lens, which is attached to the back of the source chip and whose front surface is located at the focus of the paraboloidal mirror. The collimated THz beam propagates and diffracts to 50-mm diameter, 280-mm focal length high-resistivity silicon lens, where the THz radiation is recollimated into a highly directional beam with beam diameters proportional to the wavelength and with a frequency-independent divergence typically of 25 mrad. This combination of the two silicon lenses and the optoelectronic THz source chip makes up

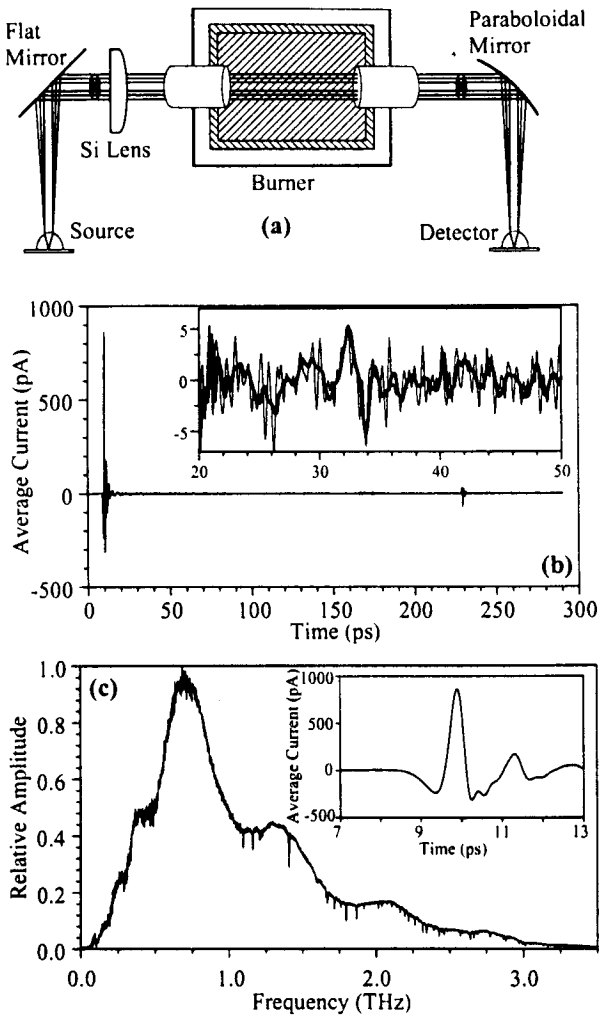

Fig. 1. (a) THz experimental system. (b) THz pulse transmitted through flame. The inset compares reference and sample scans on an expanded scale. (c) Amplitude spectrum of reference and pulse transmitted through flame. The reference THz pulse is shown in the inset on an expanded time scale.

the THz transmitter. The THz radiation transmitted through the flame is collimated by an off-axis paraboloidal mirror and silicon lens combination that focuses the THz beam on the detector and makes up the THz receiver. A coplanar stripline on semi-insulating GaAs was used as the THz source, and a 10-μm dipole antenna fabricated on ion-implanted silicon on sapphire was used as the THz detector. Optical gating was accomplished by use of a mode-locked Ti:sapphire laser that generated 70-fs excitation pulses at 820 nm.

The THz beam passes through a premixed flame stabilized on a water-cooled burner. This burner was discussed in previous publications.[6,7] The THz beam is coupled into the burner enclosure through 100-μm-thick quartz windows fused onto 5-cm-diameter quartz tubes as shown in Fig. 1(a), which permits the windows to be inserted directly into the flame, thus avoiding regions of cooler gas near the edges of the flame. The path length L through the flame was 23.2 cm. With the exception of the flame itself, the entire THz beam path is purged with air that contained less than 1-part-per-million water vapor.

The THz-TDS measurements are blind to incoherent thermal emission from high-temperature samples.[7] This is due to the phase-coherent detection and the ability to generate a well-collimated beam of THz radiation. The amplitude dynamic range of this system exceeds 5000:1. Such dynamic range is required, because the absorption of water vapor scales with temperature as approximately $T^{-5/2}$, and the amplitude absorption ($\alpha L/2$) is typically of the order of 0.25. A measured THz pulse transmitted through a propane–air flame is displayed in Fig. 1(b). The system noise level is 0.2 pA. The Fig. 1(b) inset shows an overlay of the measured THz signal transmitted through dry air (heavy line) compared with that through the flame (light line). The small and more rapid additional oscillations of the signal propagated through the flame contain all the amplitude and phase information from the water-vapor absorption. The corresponding amplitude spectrum of the pulse transmitted through the flame shown in Fig. 1(c) is obtained by a numerical Fourier transform of Fig. 1(b). The general shape of the THz spectrum is determined by the incident THz pulse [expanded in the Fig. 1(c) inset], and the much weaker oscillations that follow the initial THz pulse as shown in the Fig. 1(b) inset are responsible for the sharp absorption features. The spectrum shown in Fig. 1(c) has a useful bandwidth that extends beyond 3 THz.

One experimental limitation to the accuracy of these measurements involves the relatively long-term changes in the laser pulses and experimental alignment with consequent changes in the input THz pulses. These variations are exacerbated by the substantial change in temperature within the experiment after the burner is ignited. During an experiment we first measure the reference THz pulse (burner purged with dry air), then measure the THz pulse transmitted through the flame, and finally remeasure the reference pulse with the flame off. This sequence is repeated several times to obtain good statistics. Data for which the amplitude spectral ratio of subsequent reference pulses differs from unity by $\pm 5\%$ over the THz frequency spectrum are discarded.

3. MEASUREMENTS AND ANALYSIS

As the THz pulse propagates through the gas sample it excites a coherent ensemble of water molecules in the thermally populated rotational states. This coherent ensemble has a macroscopic polarization in the direction of the THz electric field, which is time and space coherent. As the coherent ensemble of molecules rotates with rotational frequencies determined by the rotational and vibrational quantum numbers, the ensemble emits THz radiation. This emission of THz radiation, at frequencies that correspond to a thermal distribution of rotational transitions, is seen as the oscillatory structure that follows the main THz pulse. Collisions between the various molecules of the ensemble cause dephasing and a corresponding decay of the emitted THz radiation.

This time-domain dephasing is the physical cause of line broadening in the frequency domain; rapid dephasing leads to broadened lines. Collisional broadening determines the line shape, because Doppler broadening is less than 1% of the collisional linewidth at THz frequencies,

even at the elevated temperatures in the flame. The measured linewidth is also experimentally dependent on the temporal extent of the data; i.e., ideally the data must extend far enough in time to prevent broadening from windowing of the data, which is discussed below. Thus from an experimental standpoint the measurable linewidth is dependent on the signal-to-noise ratio of the THz system; the point in time at which the signal-to-noise ratio is unity determines the maximum useful temporal extent of the data scan and hence the experimental resolution in the frequency domain. Furthermore, the frequency-domain noise scales as the square root of the temporal duration of the window. Although the peak THz signal is nearly 900 pA [Fig. 1(b)], corresponding to a signal-to-noise ratio of 4500:1, the relatively low absorption of the flame leads to a small modulation of the THz signal of the order of 5 pA as shown in the Fig. 1(b) inset. With this modulation depth the system signal-to-noise ratio limits the window over which useful data can be measured to 300 ps, following the initial THz pulse. The additional small pulses that occur approximately 200 ps after the main pulse are due to reflections of the THz pulse from the end of the coplanar transmission lines and from the surface of the silicon collimating lens. These were removed numerically prior to performing the Fourier transform to minimize frequency-domain ringing.

For a given temporal window T_W the measured time-domain data is the electric field of the THz pulse transmitted through the flame $E_{fl}(t)$, multiplied by a square window function: $W(t) = 1$ for $0 < t < T_W$; $W(t) = 0$ for $t > T_W$. The measured signal in the frequency domain is the convolution of the Fourier-transformed window function $W(\omega)$ and the complex amplitude spectrum of the THz pulse, $E_{fl}(\omega)$. The window function $W(\omega)$ is given by

$$W(\omega) = \frac{\sin(\omega T_W) + i[1 - \cos(\omega T_W)]}{\omega T_W}, \tag{1}$$

where ω is the frequency in radians per second. The FWHM of the real part of this function is $0.604/T_W$. The time-domain data were zero padded to eight times the original length, by which an interpolation in the frequency domain is performed; this does not affect T_W and does not improve the frequency resolution. For the 290-ps data scans measured here the FWHM of the sinc function is 2.1 GHz.

The ratio of the spectral data shown in Fig. 1(c) divided by the spectrum of the reference pulse determines the power absorption coefficient $\alpha(\omega)$:

$$\alpha(\omega) = -\ln\left[\frac{|E_{fl}(\omega)|^2}{|E_{ref}(\omega)|^2}\right] \Big/ L, \tag{2}$$

where L is the path length through the flame, $E_{ref}(\omega)$ is the reference spectrum, and $E_{fl}(\omega)$ is the spectrum of the THz beam propagated through the flame. The power absorption coefficient obtained by averaging four individual data scans taken under identical conditions is shown in Fig. 2. The lines marked with arrows in Fig. 2 are those for which the linewidth was determined.

To determine the actual, deconvolved linewidth $\Delta\nu$, the measured absorption lines are fit with a simplex search

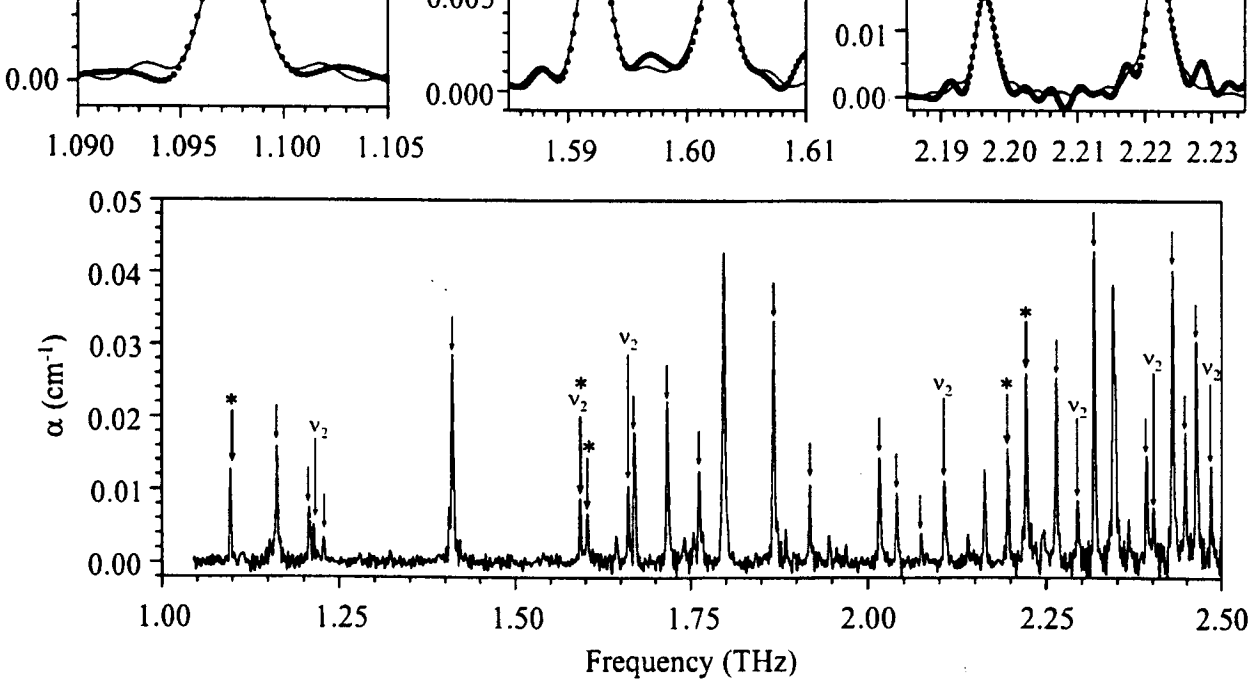

Fig. 2. Measured power absorption coefficient of active flame region. Lines marked with arrows are those for which linewidth was determined. Lines in the $\nu_2 = 1$ vibrational state are marked with ν_2 and longer arrows. Numerical fits from Eq. (3) (solid curve) and the measured data (dots) for one individual line and two pairs of lines, marked with an asterisk, appear in upper panels.

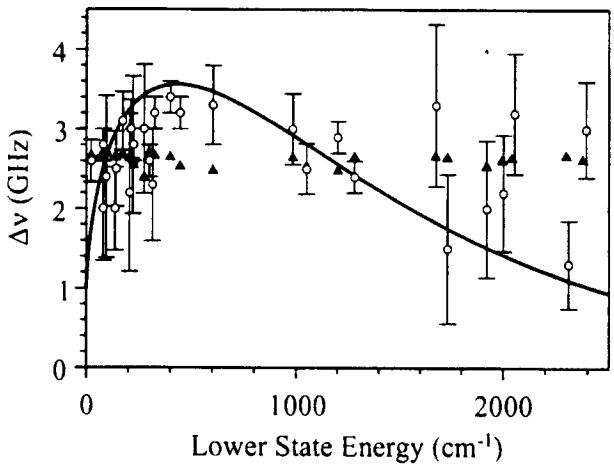

Fig. 3. Measured (open circles) and calculated (solid triangles) linewidths as a function of rotational and vibrational state energy. The error bars show estimated accuracy of the deconvolved linewidth data. Lines in the ν_2 vibrational state lie above 1594 cm^{-1}. For reference the approximate Boltzmann distribution calculated for the flame temperature of 1490 K is shown as a solid curve.

Table 1. Tabulation of Measured, Deconvolved FWHM Linewidths ($\Delta\nu_{meas}$), Transition Frequencies (ν_0), and Widths Predicted from Theory ($\Delta\nu_{theory}$)[a]

Frequency (THz)	Energy (cm^{-1})	JK_aK_c	$\Delta\nu_{theory}$ (GHz)	$\Delta\nu_{meas}$ (GHz)	Accuracy (GHz)
1.0977	136.8	3 0 3	2.68	2.0	±0.50
1.1629	173.4	3 1 2	2.72	3.1	±0.35
1.2080	275.5	4 1 3	2.68	3.0	±0.80
*1.2147	1731.9	3 0 3	2.74	1.5	±0.95
1.2287	95.2	2 1 1	2.66	2.4	±1.00
1.4108	399.5	5 1 4	2.67	3.4	±0.20
*1.5922	2000.9	5 1 4	2.70	2.2	±0.75
1.6025	222.1	4 0 4	2.65	2.8	±0.85
*1.6440	1677.1	2 1 2	2.65	3.3	±1.00
1.6608	79.5	2 1 2	2.62	2.0	±0.65
1.6697	23.8	1 0 1	2.56	2.6	±0.25
1.7170	79.5	2 1 2	2.41	2.8	±0.20
1.7621	602.8	6 2 4	2.72	3.3	±0.50
1.8680	446.5	5 2 3	2.68	3.2	±0.20
2.0163	982.9	8 2 6	2.68	3.0	±0.45
2.0407	315.8	4 2 2	2.66	2.3	±0.70
2.0745	206.3	3 2 2	2.55	2.2	±1.00
*2.1073	2392.6	7 2 5	2.49	3.0	±0.60
2.1966	212.2	3 2 1	2.66	3.0	±0.35
2.2219	325.3	5 0 5	2.54	3.2	±0.20
2.2645	224.8	4 1 4	2.49	2.8	±0.20
*2.2941	2054.0	5 2 3	2.66	3.2	±0.75
2.3181	1282.9	9 3 6	2.68	2.4	±0.20
2.3918	142.3	3 1 3	2.66	2.5	±0.45
*2.4013	1920.8	5 0 5	2.55	2.0	±0.85
2.4286	1201.9	9 2 7	2.62	2.9	±0.20
2.4476	1050.1	8 3 5	2.65	2.5	±0.30
2.4630	300.4	4 2 3	2.68	2.6	±0.20
*2.4846	2309.7	7 1 6	2.63	1.3	±0.55

[a] Lines in the $\nu_2 = 1$ manifold are marked with an asterisk. The lower rotational state energy is given in units of inverse centimeters.

fitting algorithm.[8] Well-separated individual lines or groups of closely spaced lines were fit independently of other groups of lines, but degenerate or nearly degenerate lines were not included. This minimized the number of independent variables being fit and is valid because the linewidths of the flame are considerably narrower than those at room temperature and do not overlap. The measured line profiles are fit with a numerical convolution of the real part of the Lorentz line shape[9] with the real part of the window function

$$\frac{\alpha(\omega)}{2} = \left[A\frac{\Delta\nu}{(\nu-\nu_0)^2+(\Delta\nu/2)^2}\right] * \left[\frac{\sin(\omega T_w)}{\omega T_w}\right]. \quad (3)$$

Here the asterisk represents the convolution operation and $\alpha(\omega)/2$ is the field absorption coefficient. The measured complex amplitude spectrum (from data taken over 290 ps) is equal to the convolution of the complex Lorentz line shape with that of the complex window function. In the limit in which (i) the studied absorption features are much narrower than the slowly varying spectrum of the THz reference pulse and (ii) the absorbance is small ($\alpha L \ll 1$), the measured absorption is fit well by a convolution of only the real parts of the line-shape and window functions. This approximation is valid under our experimental conditions; any error contributions to the fit of $\Delta\nu$ are much less than the experimental uncertainty. The variables A, ν_0, and $\Delta\nu$ were allowed to float to obtain the best possible fit. Even though the line centers of the transitions ν_0 are well tabulated,[10] the line center was floated to account for possible temperature shifts.

Numerical fitting was performed with several possible combinations of lines to determine the accuracy of the fits. The accuracy of the linewidth fitting is strongly dependent on the strength of the lines in the absorption spectrum. Strong lines have a numerically consistent accuracy of ±0.2 GHz for the linewidth, whereas the weaker lines in the ν_2 band are accurate to within ±1.0 GHz. The linewidth $\Delta\nu$, obtained by a fit of the measured absorption spectrum numerically by means of Eq. (3), is shown as circles in Fig. 3 with estimated accuracy of the numerical fit expressed by the error bars. The overlay of several typical fits (solid curve) with experimental data (dots) is shown expanded for visibility as the upper panels in Fig. 2. The numerical fits shown were performed individually for a single line at 1.097 THz, a pair of lines at 1.592 and 1.603 THz, and the pair at 2.197 and 2.222 THz. The fit parameters ν_0, $\Delta\nu$ and the accuracy of $\Delta\nu$ are given in Table 1 along with the energy and quantum numbers of the lower state of the rotational transition. The lines in the $\nu_2 = 1$ vibrational state are indicated with an asterisk.

4. DISCUSSION

In the samples of high-temperature water vapor used here the two dominant broadening mechanisms are collisions with other water molecules and collisions with nitrogen. The total linewidth is inversely related to the dephasing time τ by $\Delta\nu = 1/\pi\tau$. The overall dephasing

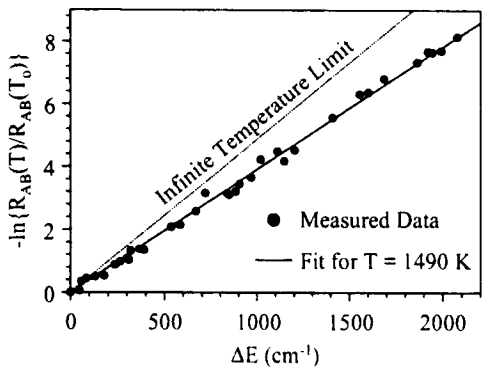

Fig. 4. Ratio of absorption peaks measured in flame to those calculated at room temperature. Fitting the line slope determines sample temperature.[6]

time of water molecules in the flame is determined by collisions between all gas species X with concentration $[\%\ X]$ and dephasing time τ_x:

$$\frac{1}{\tau} = \frac{[\%\ CO_2]}{\tau_{CO_2}} + \frac{[\%\ H_2O]}{\tau_{H_2O}} + \frac{[\%\ N_2]}{\tau_{N_2}} + \frac{[\%\ O_2]}{\tau_{O_2}}. \tag{4}$$

For the propane–air ratios used to generate our sample the relative concentrations are 73 ± 4% N_2, 9 ± 0.5% CO_2, 4 ± 0.2% O_2, and 13 ± 0.7% H_2O. The species CO_2 and O_2 do not contribute much to the overall collisional dephasing, owing to their small dipole moments (small collisional cross sections) and relatively low concentrations. However, for completeness, we compare our data with theoretically calculated linewidths, including contributions from these species.

The linewidth of a particular rotational state transition at temperatures above 250 K has a temperature dependence of the form $\Delta\nu(T) = \Delta\nu(T_0)(T/T_0)^{-n}$, with the exponent n typically between 0.5 and 1. T_0 is a known reference temperature, usually 300 K. This power-law dependence is a result of the T^{-1} dependence of the number density, the $T^{1/2}$ dependence of the velocity, and the T^{-m} dependence of the collisional cross section, which is dependent on the details of the molecular interactions during a collision.[11]

To determine temperatures within the flame, we compare measured absorption line strengths within our flame with those calculated from tabulated data[10] at a known temperature. Plotting the natural logarithm of the measured ratio of two absorption lines at the known and unknown temperatures compared with the difference in lower state energies allows for a graphical determination of the flame temperature,[6] as shown in Fig. 4. Twenty-one well-separated lines were used to measure a temperature of 1490 K, determined from the slope of the line in Fig. 4.

Because of the inherent technical difficulties in accessing this spectral region, particularly for high-temperature samples, there is minimal experimental data on water-vapor absorption at high temperatures. The existing body of data includes foreign gas broadening on the $3_{1,3} \rightarrow 2_{2,0}$ transition at 183 GHz (6.1 cm^{-1}) from 80 K to 600 K,[12] diode laser measurements in the ν_2 band[13] near 2000 cm^{-1}, and emission measurements[14–16] of ν_2-band transitions in the 800–1900-cm^{-1} range at 2000 K. None of these studies cover the 33–83-cm^{-1} spectral range.

Theoretical work on collisional broadening is more complete, covering the entire FIR spectral range for X–H_2O collisions with X = N_2, O_2, CO_2, and H_2O.[17–20] We compare our measurements with the calculations of Delaye *et al.*,[20] because they include all the species present in our flame environment. These theoretical results are used to calculate the individual FWHM at the measured temperature of 1490 K for our flame gas mixture for each of the rotational transitions that are measured experimentally. The theoretically calculated linewidths are overlaid on our measurements of $\Delta\nu$ as triangles in Fig. 3.

The circles in Fig. 3 show that the measured linewidths $\Delta\nu$ [deconvolved from the experimental data by means of Eq. (3)] have a strong dependence on the rotational state energy, appearing to peak near an energy of 600 cm^{-1}. The overall linewidth dependence on energy is much more pronounced than was calculated[20] and is similar to the peak of the Boltzmann distribution shown for reference as a solid curve in Fig. 3. The correlation between energy-dependent linewidth and the Boltzmann distribution is similar to that observed previously with THz-TDS for room-temperature methyl halides.[9] Such dependence has been calculated theoretically for H_2O–H_2O broadening at 1800 K[20] but is not expected for the multicomponent gas mixture of the flame environment.

We obtain reasonable agreement of the other two lineshape fitting parameters, the line strength A, and the center frequency ν_0, with tabulated values.[10] Numerical fits of line center agreed within ±0.4 GHz in the worst case and more typically within ±0.2 GHz to tabulated values. The line centers ν_0 fit to the experimental data are tabulated in Table 1. We do not observe any temperature shifts of these lines.

The line-strength fit by the parameter A in Eq. (3) is in general in good agreement with tabulated values. However, extracting the line strength from the experimentally measured peak absorption is dependent on the ability to accurately measure temperature and linewidth. The measured line strength is compared with tabulated values[10] at 300 K, by use of the approximation of a $T^{3/2}$ dependence for the partition function of nonlinear molecules. The temperature determined by the fit to the data in Fig. 4 is estimated to be accurate to +20%–10%. The larger uncertainty on the high-temperature side is due to the fact that the line slope changes more gradually as the temperature approaches the infinite limit, as shown in Fig. 4. The measured absorption coefficient from which line strength is extracted is also dependent on uncertainties in $\Delta\nu$ of ±10% to ±40%, depending on the strength of the absorption line, baseline noise of ±0.001 cm^{-1}, and on the estimate of the number density of water molecules determined by measured gas flow rates (±5%) and the T^{-1} number density dependence on temperature. From this the overall line-strength uncertainty is predicted to be +50%–30% for the strong lines and +65%–50% for the weak lines. All measured line strengths agree with calculations within these uncertainties. However, the difference between the measured and the calculated line strength increases with increasing frequency.

This variation was observed previously[7] and attributed to the linewidth, which was unknown at that time. This discrepancy remains with the current data and remains unexplained. The difference between theory and experiment might be due to a systematic error in temperature determination, because the overall $T^{-5/2}$ dependence of line strength with temperature strongly affects the calculated absorption spectrum. Extrapolating line strengths from 300-K data to the high temperatures by means of an approximate partition function might also account for the discrepancies.

5. SUMMARY AND CONCLUSIONS

What we believe to be the first absorption linewidth measurements of high-temperature water vapor in the far-IR (FIR) region of the spectrum have been reported. The experimental technique of THz-TDS permits simultaneous measurement of many lines over a broad frequency region to determine the line center, strength, and width of pure rotational transitions from 1.0 to 2.5 THz (33 to 83 cm^{-1}) for molecules in both ground and $\nu_2 = 1$ vibrational states. The measured linewidths agree in magnitude with calculated values at the measured temperature; however, contrary to predictions, a pronounced energy dependence was observed. No temperature shift of line centers was observed, and line strengths were in reasonable agreement with tabulated values. The demonstrated ability of THz-TDS to measure linewidths of pure rotational transitions in hot samples will be extended to other samples and gas mixtures. This will expand the minimal experimental data on the temperature dependence of linewidth[21]:

$$\Delta\nu(T) = \Delta\nu(T_0)[T_0/T]^n \quad (5)$$

to permit measurements of the exponent n. Because n is typically of the order of 0.6, measurements over a broad range of temperatures are required for accurate determination of this exponent.

ACKNOWLEDGMENTS

This work was supported in part by the National Science Foundation under grants PHY-9422952 and PHY-9731201.

R. A. Cheville can be reached by telephone at 405-744-6625, and by e-mail at kridnix@thzsun.ecen.okstate.edu. D. Grischkowsky can be reached by e-mail at grischd@master.ceat.okstate.edu.

REFERENCES

1. D. J. Perkey, *Atmospheric Water Vapor*, A. Deepak, T. D. Wilkerson, and L. H. Ruhnke, eds. (Academic, New York, 1980), pp. 513–526.
2. H. A. Gebbie, *Atmospheric Water Vapor*, A. Deepak, T. D. Wilkerson, and L. H. Ruhnke, eds. (Academic, New York, 1980), pp. 133–201.
3. O. L. Polyansky, N. F. Zobov, S. Viti, J. Tennyson, P. F. Bernath, and L. Wallace, "Water on the Sun: line assignments based on variational calculations," Science **277**, 346–348 (1997).
4. L. Wallace, P. Bernath, W. Livingston, K. Hinkle, J. Busler, B. Guo, and K. Zhang, "Water on the Sun," Science **268**, 1155–1158 (1995).
5. D. A. Neufeld and G. J. Melnick, "Excitation of millimeter and submillimeter water masers," Astrophys. J. **368**, 215–230 (1991).
6. R. A. Cheville and D. Grischkowsky, "Far-infrared terahertz time-domain spectroscopy of flames," Opt. Lett. **20**, 1646–1648 (1995).
7. R. A. Cheville and D. Grischkowsky, "Observation of pure rotational absorption spectra in the ν_2 band of hot H_2O in flames," Opt. Lett. **23**, 531–533 (1998).
8. T. Mathworks, *Matlab Reference Guide* (The Math Works Inc., Natick, Mass., 1995).
9. H. Harde, R. A. Cheville, and D. Grischkowsky, "Terahertz studies of collision-broadened rotational lines," J. Phys. Chem. A **101**, 3646–3660 (1997).
10. H. M. Pickett, R. L. Poynter, E. A. Cohen, M. L. Delitsky, J. C. Pearson, and H. S. P. Muller, "Submillimeter, millimeter, and microwave spectral line catalog," J. Quant. Spectrosc. Radiat. Transf. **60**, 883–890 (1998).
11. C. H. Townes and A. L. Schawlow, *Microwave Spectroscopy* (Dover, New York, 1975).
12. T. M. Goyette and F. C. De Lucia, "The pressure broadening of the $3_{1,3}$–$2_{2,0}$ transition of water between 80 and 600 K," J. Mol. Spectrosc. **143**, 346–348 (1990).
13. J. M. Hartmann, J. Taine, J. Bonamy, B. Labini, and D. Robert, "Collisional broadening of rotation-vibration lines for asymmetric top molecules. II. H_2O diode laser measurements in the 400–900 K range, calculations in the 300–2000 K range," J. Chem. Phys. **86**, 144–156 (1987).
14. J.-Y. Mandin, V. Dana, C. Camy-Peyret, and J.-M. Flaud, "Collisional widths of pure rotational transitions of H_2O from Fourier-transform flame spectra," J. Mol. Spectrosc. **152**, 179–184 (1992).
15. V. Dana, J.-Y. Mandin, C. Camy-Peyret, J.-M. Flaud, J.-P. Chevillard, R. L. Hawkins, and J.-L. Delfau, "Measurements of the collisional linewidth in the ν_2 band of H_2O from Fourier-transformed flame spectra," Appl. Opt. **31**, 1928–1936 (1992).
16. V. Dana, J.-Y. Manding, C. Camy-Peyret, J.-M. Flaud, and L. S. Rothman, "Rotational and vibrational dependences of collisional linewidth in the $n\nu_2 - (n-1)\nu_2$ hot bands of H_2O from Fourier-transform flame spectra," Appl. Opt. **31**, 1179–1184 (1992).
17. P. W. Rosenkranz, "Pressure broadening of rotational bands. II. Water vapor from 300 to 1100 cm^{-1}," J. Chem. Phys. **87**, 163–170 (1987).
18. R. R. Gamache and L. S. Rothman, "Temperature dependence of N_2-broadened halfwidth of water vapor: the pure rotational and ν_2 bands," J. Mol. Spectrosc. **128**, 360–369 (1988).
19. R. R. Gamache and R. W. Davies, "Theoretical calculations of N_2-broadened halfwidths of H_2O using quantum Fourier transform theory," Appl. Opt. **22**, 4013–4019 (1983).
20. C. Delaye, J.-M. Hartmann, and J. Taine, "Calculated tabulations of H_2O line broadening by H_2O, N_2, O_2, and CO_2 at high temperature," Appl. Opt. **28**, 5080–5087 (1989).
21. S. D. Gasster, C. H. Townes, D. Goorvitch, and F. P. J. Valero, "Foreign-gas collision broadening of the far-infrared spectrum of water vapor," J. Opt. Soc. Am. B **5**, 593–601 (1988).